



## Reversible and Irreversible Deformation Mechanisms of Composite Graphite Electrodes in Lithium-Ion Batteries

E. M. C. Jones,<sup>a,b,\*</sup> Ö. Ö. Çapraz,<sup>b,c,d</sup> S. R. White,<sup>b,c</sup> and N. R. Sottos<sup>b,d,z</sup>

<sup>a</sup>Department of Mechanical Science and Engineering, University of Illinois at Urbana-Champaign, Urbana, Illinois 61802, USA

<sup>b</sup>Beckman Institute, University of Illinois at Urbana-Champaign, Urbana, Illinois 61802, USA

<sup>c</sup>Department of Aerospace Engineering, University of Illinois at Urbana-Champaign, Urbana, Illinois 61802, USA

<sup>d</sup>Department of Materials Science and Engineering, University of Illinois at Urbana-Champaign, Urbana, Illinois 61802, USA

Repeated charge and discharge of graphite composite electrodes in lithium-ion batteries cause cyclic volumetric changes in the electrodes, which lead to electrode degradation and capacity fade. In this work, we measure in situ the electrochemically-induced deformation of graphite composite electrodes. The deformation is divided into a reversible component and an irreversible component. Reversible expansion/contraction of the composite electrodes is correlated with localized changes in graphite layer spacing associated with different graphite-lithium intercalation compounds. Phase transitions between different intercalation compounds are manifested during galvanostatic cycling as peaks in the derivative of capacity with respect to voltage; these peaks correspond remarkably well with peaks in the derivative of strain with respect to voltage. Irreversible electrode deformation is correlated with deposition of electrolyte decomposition products on graphite particles during the formation and growth of the solid electrolyte interphase (SEI). Both the irreversible capacity and the irreversible strain developed during galvanostatic cycling increase with increasing electrode surface area and increasing cycling time. During a potentiostatic voltage hold at 0.5 V vs  $\text{Li}^{+0}$ , in which electrolyte decomposition is the dominating electrochemical reaction, both the capacity and the electrode strain increase proportional to the square root of time. Interestingly, the choice of polymer binder, either carboxymethyl cellulose (CMC) or polyvinylidene fluoride (PVdF), has a significant influence on the irreversible electrode deformation, suggesting that the formation and growth of the SEI layer is influenced by the polymer binder.

© 2016 The Electrochemical Society. [DOI: 10.1149/2.0751609jes] All rights reserved.

Manuscript submitted March 29, 2016; revised manuscript received June 24, 2016. Published July 14, 2016.

Porous, particulate, composite electrodes comprised of particles of graphite as the active material, a nanoscale conductive additive such as carbon black, and a polymeric binder, are the most common anodes for commercial lithium-ion batteries.<sup>1</sup> During battery charging, lithium ions intercalate between graphite layers, forming a series of well-ordered graphite-lithium intercalation compounds: dilute stage I ( $\text{LiC}_x$ ,  $x < 24$ ), stage IV ( $\text{LiC}_{24}$ ), stage III ( $\text{LiC}_{18}$ ), dilute stage II ( $\text{LiC}_{18}$ ), stage II ( $\text{LiC}_{12}$ ), and stage I ( $\text{LiC}_6$ ).<sup>2,3</sup> The Roman numerals denote the number of graphite layers associated with each layer of intercalated lithium. Fully intercalated layers contain one lithium atom per six carbon atoms, while dilute layers (denoted with a capital D, i.e. DI and DII) contain less than one lithium atom per six carbon atoms.

Each stage of intercalation compounds has a characteristic graphite layer spacing,<sup>2-5</sup> and changes in the layer spacing at the atomic scale are translated through multiple length scales. At the microscale, the volumetric expansion of fully intercalated (stage I) polycrystalline graphite particles has been calculated as ca. 10% from density functional theory, with experimental X-ray diffraction measurements of ca. 13% closely agreeing.<sup>4</sup> In prior work,<sup>6</sup> we measured the dilation of free-standing composite graphite electrodes (not adhered to a current collector). We found that fully lithiated electrodes develop approximately 1.5–2.0% linear strain, which corresponds to ca. 4.5–6.1% volumetric strain assuming isotropic expansion. By releasing the constraint of the substrate, we were able to achieve highly repeatable measurements that compared well to mechanics models.

In commercial batteries, composite electrodes are constrained by current collectors, which limit macroscale expansion and contraction of the electrodes.<sup>7,8</sup> As a result, the microscale particle expansion causes stresses to develop in the electrodes.<sup>9</sup> Using substrate curvature techniques, Sethuraman et al.<sup>10</sup> calculated the stress development in graphite-based composite electrodes during galvanostatic cycling. Mukhopadhyay et al.<sup>11,12</sup> found that electrodes comprised of graphitic carbon with basal planes aligned parallel to a substrate developed significantly less stress than electrodes com-

prised of graphitic carbon with basal planes aligned perpendicular to a substrate.

Electrochemically-induced expansion and concurrent stress development has been investigated in other electrode materials for lithium-ion batteries. Early work focused on observing expansion and fracture of high-capacity anode materials, such as silicon and tin.<sup>13-15</sup> More recently, Sethuraman et al. calculated the stress in both model thin film silicon electrodes<sup>16</sup> as well as silicon-based composite electrodes.<sup>17</sup> Expanding to 3D measurements, Gonzalez et al.<sup>18</sup> characterized the microstructural evolution of silicon composite electrodes during the initial lithiation using X-ray computed tomography. Cathode materials have been investigated by Eastwood et al.,<sup>19</sup> who tracked the dilation and motion of manganese oxide cathode particles on multiple length scales using X-ray computed tomography and digital volume correlation.

Because of the low working voltage of graphite-based and silicon-based anodes ( $< 0.3$  V vs  $\text{Li}^{+0}$ ), electrolyte species, including carbonate solvents, lithium salts, and impurities (e.g. water), reduce irreversibly at the anode surface when lithium-ion batteries are charged for the first time.<sup>20</sup> These reductive decomposition reactions begin at ca. 0.8 V vs  $\text{Li}^{+0}$  and continue to take place down to 0 V vs  $\text{Li}^{+0}$ .<sup>21</sup> Electrolyte decomposition products are deposited onto the surface of the anode, forming a thin layer, ca. 10–100 nm thick, called the solid-electrolyte interphase (SEI).<sup>20,22</sup> Ideally, the SEI passivates the electrode surface, preventing further electrolyte decomposition. However, particle fracture induced by cyclic fatigue during repeated charge / discharge cycles exposes fresh anode surfaces to the electrolyte.<sup>23-30</sup> Lithium ions consumed during continuous electrolyte decomposition is one of the primary causes of capacity fade associated with the anode.<sup>20</sup> Thus, the electrochemically-induced mechanical response of the electrode (i.e. dilation, stress development, and fracture) is directly connected to the longevity and reliability of lithium-ion batteries.

Mukhopadhyay and Tokranov et al.<sup>31,32</sup> correlated irreversible stress development in oriented graphitic carbon electrodes with the formation and growth of the SEI layer. They found that the irreversible stresses in the electrode due to SEI formation were of the same order of magnitude as the reversible stresses due to lithium intercalation/deintercalation. Tavassol et al.<sup>33</sup> found that the SEI formed

\*Electrochemical Society Student Member.

<sup>z</sup>E-mail: n-sottos@illinois.edu

on a model gold electrode also resulted in irreversible stress generation. These results showed for the first time that surface processes at the electrode/electrolyte interface directly affect the mechanical response of the electrodes.

In the present work, we investigate the strain response of free-standing composite graphite electrodes (i.e. electrodes not adhered to a substrate) during electrochemical cycling. Measurements of the free expansion and contraction of electrodes provide a model system for understanding the mechanical response of electrodes due to electrochemical processes alone, without influence of constraint applied by current collectors or battery packaging. Through these strain measurements, two principle deformation mechanisms are identified. Reversible macroscale deformation of composite graphite electrodes is correlated with changes in the graphite layer spacing at the atomic scale as different graphite-lithium intercalation compounds are formed. Irreversible electrode deformation is correlated with the formation and growth of the solid-electrolyte interphase (SEI). Finally, the polymer binder utilized in the composite electrodes is found to influence both the reversible and the irreversible electrode deformation during electrochemical cycling and SEI formation and growth.

## Experimental

**Electrode fabrication.**—Free-standing composite graphite electrodes were fabricated using the following procedure. First, one of two polymer binders was dissolved in a solvent: either carboxymethyl cellulose (CMC, average  $M_w \sim 700,000$ , DOS 0.8–0.95, Sigma-Aldrich) in deionized water in a 1:100 wt ratio, or polyvinylidene fluoride (PVdF, Kynar, Arkema) in N-methyl-2-pyrrolidone (NMP, anhydrous, 99.5%, Sigma Aldrich) in a 1:75 or 1:50 wt ratio. Next, a prescribed amount of graphite (<20  $\mu\text{m}$ , Sigma-Aldrich) and carbon black (CB, 100% compressed, 99.9+ % pure, Alfa Aesar) were added to the binder solution so that the mass ratio of graphite to carbon black ranged from 9:0 (i.e. all graphite, no carbon black) to 0:9 (i.e. all carbon black, no graphite), with the binder content remaining constant at 10 wt%. Some suspensions were mixed with a magnetic stir rod for several days and others were mixed using a homogenizer (Model 15007ST, Omni) at approximately 7,500 RPM for 1 hour. The mixing protocol had no noticeable influence on the electrochemical behavior or the strain response of the electrodes. The resulting electrode slurry was spread onto a copper foil substrate (9  $\mu\text{m}$  thick, 99.99%, MTI) using a doctor blade to control the slurry height. After the electrode was dry, it was carefully peeled off of the copper substrate, creating a free-standing electrode 90–100  $\mu\text{m}$  thick. Finally, fluorescent silica nano-particles were spin-cast onto the electrode surface to create a speckle pattern for digital image correlation (Strain measurement technique section). Then the electrode was cut into rectangular pieces, approximately  $3 \times 7$  mm, with a typical mass of 1.5–3.0 mg. The density of the electrodes was estimated to be in the range of 0.9–1.2  $\text{mg mm}^{-3}$  for electrodes with an 8:1:1 wt ratio of graphite, carbon black, and either CMC or PVdF binder.

**Strain measurement technique.**—In prior work,<sup>6</sup> a custom battery half-cell was designed that allowed for optical access to a nearly unconstrained working electrode during electrochemical cycling against a lithium metal counter electrode (Fig. S1a in the supporting information). In this work, a free-standing composite graphite electrode (i.e. not adhered to a current collector) served as the working electrode, and it was cantilevered off the edge of a stainless steel substrate. Spot welds created an electrical connection between the electrode and the battery circuit and fixed the electrode to the stainless steel substrate during cycling. On the opposite free edge of the electrode, a polymer support with a thin gap (approximately 200  $\mu\text{m}$ ) limited the out-of-plane deflection of the electrode while allowing free in-plane expansion and contraction (Fig. S1b in the supporting information). The region of the electrode between the two supports was nearly unconstrained, and it was on this unconstrained region that strain measurements were performed.

Displacements and strains in the electrode were measured by digital image correlation (DIC), an optical, non-contact, full-field strain measurement technique. A well-correlated speckle pattern for DIC was created by spin casting fluorescent silica nano-particles onto the electrode surface.<sup>6,34–36</sup> During electrochemical cycling, a laser (CrystaLaser, 532 nm, 75 mW) illuminated the electrode surface with an elliptical spot size of ca.  $4 \times 5$  mm to excite the fluorescent particles, and the emitted fluorescent light was captured with a CCD sensor (EXi Aqua camera, QImaging). Images were captured every 10 minutes of a  $2.5 \times 3.0$  mm region of interest (ROI), located between the two supports, immediately adjacent to the spot welds (Fig. S1b in supporting information).

The effective strain due to free expansion and contraction of the electrode was represented by the rotationally invariant equivalent strain,  $E_{eqv}$ , defined by:

$$E_{eqv} = \left[ \frac{3}{2} \left( E_{ij} E_{ij} - \frac{1}{3} E_{mm} E_{nn} \right) \right]^{1/2}, \quad [1]$$

where  $E_{ij}$  are the components of the two-dimensional, finite strain tensor, and repeated indexes imply summation. The strain field was isotropic and homogeneous approximately 1.0 mm away from the spot welds.<sup>6</sup> For each image captured during cycling, the equivalent strain was averaged over a vertical line in the center of the region of interest, approximately 1.5 mm away from the spot welds.

**Electrochemical cycling.**—Composite graphite working electrodes were cycled against a lithium metal counter electrode (0.75 mm thick, 99.9%, Alfa Aesar) in an electrolyte comprised of 1 M  $\text{LiClO}_4$  (battery grade, dry, 99.99%, Sigma Aldrich) in a 1:3 vol. ratio mixture of ethylene carbonate (EC, anhydrous, 99%, Sigma Aldrich) and dimethyl carbonate (DMC, anhydrous, >99%, Sigma Aldrich). The custom battery cell was assembled in an argon atmosphere with  $\text{O}_2$  and  $\text{H}_2\text{O}$  levels below 5 ppm and then brought into atmospheric conditions for testing. Within approximately 30 minutes of battery cell assembly, the cell was placed in the experimental setup and allowed to rest at open circuit potential for five hours while images were captured of the fluorescent particles on the electrode surface. This five-hour rest period allowed the cell to reach mechanical equilibrium. The reference point for all strain measurements was taken after this rest period, just prior to cycling. A brief discussion of the rest period is provided in the supporting information (Sec. S2).

**Galvanostatic cycling.**—Galvanostatic cycling tests were performed between 2 V and 10 mV vs.  $\text{Li}^{+0}$  on an Arbin potentiostat/galvanostat. In this work, discharge of the half cell (i.e. lithium ions moving from the lithium metal counter electrode to the graphite working electrode) is referred to as “lithiation,” and charge of the half cell (i.e. lithium ions moving from the graphite working electrode to the lithium metal counter electrode) is referred to as “delithiation.” Images of the fluorescent particles on the electrode surface were captured every 10 minutes. Therefore, each constant current charge/discharge step was followed by a constant voltage hold of 11 minutes in order to capture an image at the end of each lithiation and delithiation portion of cycling. Following the constant voltage step, the cell rested for 10 seconds (no applied current or voltage) to allow the potentiostat/galvanostat to switch smoothly to the next step. The C-rates reported were calculated using the theoretical capacity of graphite,  $Q_g = 372$   $\text{mA h g}^{-1}$ ,<sup>37</sup> and the mass of graphite in the electrode,  $m_g$ :

$$\text{C-rate} = \frac{Q_g m_g}{I}, \quad [2]$$

where  $I$  is the current used in the constant current portion of cycling. All capacities reported were normalized by the mass of the graphite, unless otherwise noted.

**Potentiostatic test.**—To explore the effect of electrolyte decomposition on electrode deformation, we designed a test in which electrolyte reduction was the dominating electrochemical reaction.

Electrodes with a mass ratio of 8:1 graphite to binder (no carbon black) were held potentiostatically at a voltage of 0.5 V vs  $\text{Li}^{+/0}$  for a certain amount of time while the current and strain responses were monitored. The voltage of 0.5 V vs  $\text{Li}^{+/0}$  was below the threshold for reduction of electrolyte solvents (ca. 0.8 V vs  $\text{Li}^{+/0}$ ),<sup>21</sup> but above the threshold for lithium intercalation into graphite (ca. 0.3 V vs  $\text{Li}^{+/0}$ ).<sup>2</sup> Electrodes were fabricated without carbon black to avoid any contribution to the capacity from lithium intercalation into carbon black, which occurs at voltages lower than ca. 1.5 V vs  $\text{Li}^{+/0}$ .<sup>2</sup> Therefore, all capacity gained during this voltage hold was directly associated with irreversible electrolyte decomposition.

**Electrode imaging.**—Select electrodes were imaged in a scanning electron microscope before and after electrochemical cycling. After cycling, the custom battery cell was disassembled in an argon atmosphere and the electrode was rinsed with dimethyl carbonate to remove residual electrolyte salts from the electrode surface. The electrode was then brought into atmospheric conditions, and further rinsed with ethanol before imaging.

## Results and Discussion

**Representative electrode response during galvanostatic cycling.**—Fig. 1a shows the representative electrochemical behavior of a graphite composite electrode (8:1:1 wt ratio of graphite, carbon

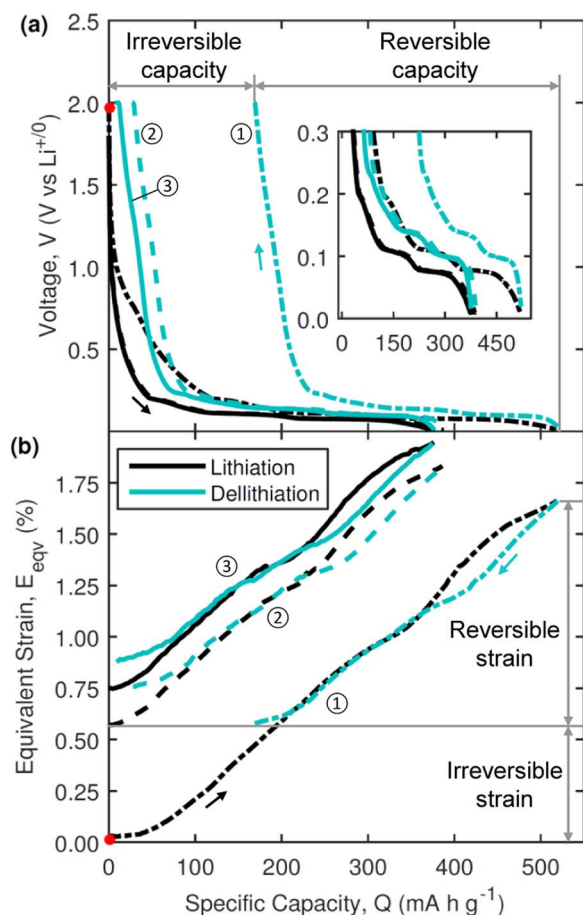


**Figure 1.** Electrochemical and mechanical response of a graphite composite electrode during galvanostatic cycling. The electrode had a composition of 8:1:1 wt ratio of graphite, carbon black and CMC binder, and was cycled at C/20 rate for three cycles. Circled numbers denote cycle number. (a) Representative electrochemical response and (b) representative strain response. The reversible and irreversible portions of the capacity and strain responses are demarcated for the first cycle.

black, and CMC binder) cycled galvanostatically at C/20 rate for three cycles. The start of the test is marked by a red circle, at the open circuit potential of 2.2 V vs  $\text{Li}^{+/0}$ . The lithiation portion of the first cycle showed an artificially high specific capacity due to the decomposition of the electrolyte,<sup>20</sup> resulting in 167 mA h  $\text{g}^{-1}$  of irreversible capacity. The inefficiency of the cell (i.e. the difference between the lithiation capacity and the delithiation capacity) indicated continued electrolyte decomposition on cycles two and three, though to a smaller extent than the main decomposition on the first cycle. The cell achieved a reversible capacity of approximately 360 mA h  $\text{g}^{-1}$ , which is close to the theoretical capacity of graphite (372 mA h  $\text{g}^{-1}$ ),<sup>37</sup> indicating that the electrode cycled well in the custom battery cell.

The strain response of the graphite composite electrode is shown in Fig. 1b. The start of the test is marked by a red circle, at zero strain and zero capacity. As lithium intercalated into the electrode, the capacity increased and the strain increased (black curve), indicating expansion of the electrode. As lithium was removed from the electrode, the capacity decreased and the electrode contracted (blue curve). After the first cycle, the electrode did not contract to its original size, resulting in 0.56% irreversible strain. The cumulative irreversible strain increased with additional cycles. The average reversible strain of the electrode was 1.1%, which is in good agreement with analytical predictions.<sup>6</sup>

In the following sections, the reversible and irreversible deformation of graphite composite electrodes is investigated in detail, and two main deformation mechanisms are elucidated (Fig. 2). Namely, reversible deformation is correlated with changing spacing between graphite layers as lithium is intercalated and deintercalated from graphite. Irreversible deformation is correlated with the formation and growth of the SEI layer.

**Reversible behavior: graphite-lithium intercalation compounds.**—During galvanostatic cycling, transitions between graphite-lithium intercalation compounds are manifested as voltage plateaus (inset of Fig. 1a) or equivalently as peaks in the derivative of capacity with respect to voltage. Through simultaneous X-ray diffraction measurements of the graphite layer spacing and galvanostatic cycling of composite graphite electrodes, Dahn et al.<sup>2,3</sup> associated four of the five expected phase transitions between different intercalation compounds with specific peaks in the capacity derivative. The voltage values where the peaks occur and the corresponding phase transitions are listed in Table I for reference.

Following the work of Dahn et al., we present the derivative of capacity with respect to voltage of a graphite composite electrode in Fig. 3a. Four peaks were observed in the capacity derivative, labeled  $A_i$ ,  $B_i$ ,  $C_i$ , and  $D_i$ , where the subscript  $i$  denotes either the lithiation portion of cycling ( $i = L$ ) or the delithiation portion of cycling ( $i = D$ ). The peaks in the capacity derivative in Fig. 3a were associated with specific phase transitions of intercalation compounds through correlation of the location and relative magnitude of the peaks with those shown by Dahn et al.<sup>2,3</sup> The voltages at which the peaks in the capacity derivative occurred, averaged over cycles 2–3, are listed in Table I with the corresponding phase transitions.

The corresponding derivative of the strain with respect to voltage of a graphite composite electrode is presented in Fig. 3b. The voltages at which the peaks of the strain derivative occurred, averaged over cycles 2–3, are listed in Table I. The peaks in the strain derivative corresponded remarkably well with the peaks in the capacity derivative, both in terms of location and relative magnitude. This correspondence indicates that the reversible strain developed at the macroscale in the graphite composite electrode was directly related to the atomic-scale changes in graphite layer spacing associated with different graphite-lithium intercalation compounds. This mechanism of reversible deformation is illustrated schematically in Fig. 2.

**Irreversible behavior: electrolyte decomposition.**—Scanning electron micrographs of the edge of a graphite composite electrode before and after galvanostatic cycling are presented in Fig. 4. The images of the cycled electrode clearly reveal new material coating

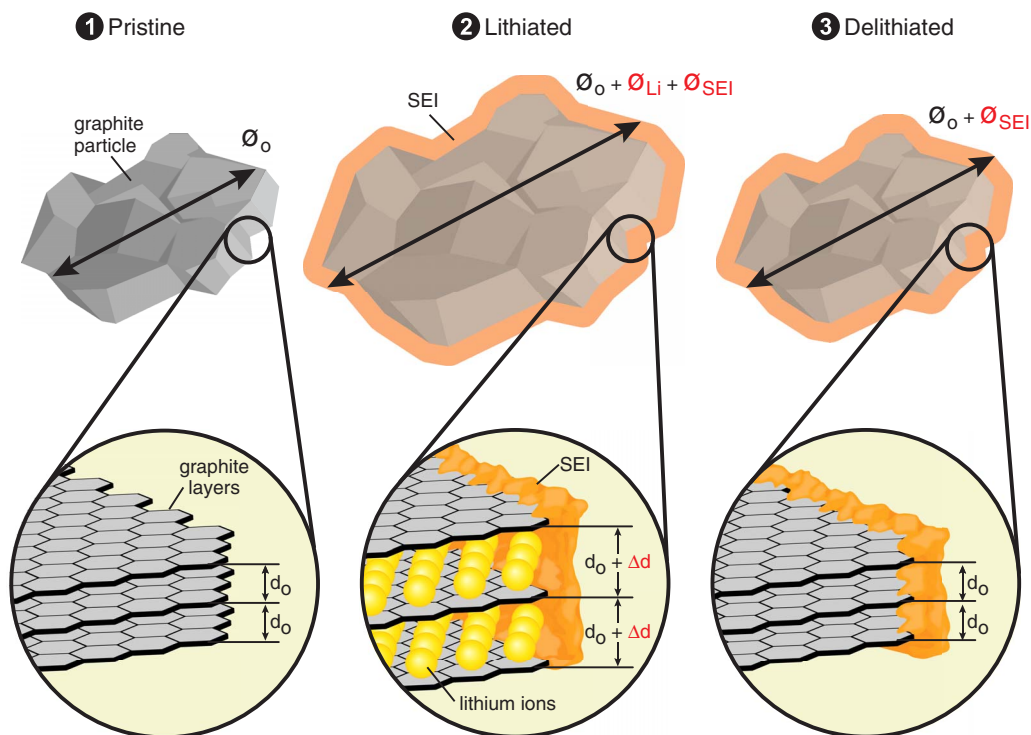


**Figure 2.** Schematic depicting mechanisms of reversible and irreversible deformation of graphite electrodes. (1) A pristine graphite particle has an initial size of  $\phi_o$ , determined by the characteristic layer spacing of  $d_o$  between graphite layers. (2) Lithium intercalation causes the graphite layer spacing to increase by  $\Delta d$  at the atomic scale, which is translated to the microscale as an overall size increase of the graphite particle by  $\phi_{Li}$ . Deposition of electrolyte reduction products on the surface of the graphite particle during the formation of the solid-electrolyte interphase (SEI) causes a further increase in the graphite particle size of  $\phi_{SEI}$ . (3) Upon delithiation, deformation due to lithium intercalation is recovered, but the increase in the particle size due to SEI formation is irreversible.

the surfaces of the graphite and carbon black particles. In control images (Fig. S3 in the supporting information) of an electrode that was soaked in electrolyte for the equivalent amount of time, but was not cycled, no coating was observed. Therefore, we believe the film on the cycled electrodes is the solid-electrolyte interphase (SEI) composed of electrolyte decomposition products deposited on the electrically-conductive surfaces of the graphite composite electrode during electrochemical cycling.

The formation of the SEI layer is the primary source of irreversible capacity loss associated with graphite electrodes.<sup>20</sup> As shown in Fig. 1, both the irreversible capacity and the irreversible strain of free-standing composite graphite electrodes accumulated primarily during the first cycle of galvanostatic cycling, with smaller increases during later cycles. Thus, the irreversible strain is correlated with the irreversible capacity associated with SEI formation during galvanostatic

cycling. Mukhopadhyay and Tokranov et al.<sup>31,32</sup> similarly correlated irreversible stress development in graphitic carbon electrodes with SEI formation, and Tavassol et al.<sup>33</sup> also correlated irreversible stress with SEI formation on model gold electrodes.

In order to explore the relationship between irreversible capacity and irreversible strain further, we systematically varied the composition of the electrodes, investigating electrodes with 9:0:1, 8:1:1, 6:3:1, and 0:9:1 wt ratios of graphite, carbon black, and CMC binder. By varying the ratio of graphite to carbon black in the electrode, we effectively varied the specific surface area of the electrically-conductive portion of the electrode,  $\beta_{elec}$ , which is approximated as:

$$\beta_{elec} = M_{f,g}\beta_g + M_{f,cb}\beta_{cb} \quad [3]$$

where  $\beta_g$  is the specific surface area of graphite (ca.  $10 \text{ m}^2 \text{ g}^{-1}$ ),<sup>38</sup>  $\beta_{cb}$  is the specific surface area of carbon black (ca.  $60\text{--}80 \text{ m}^2 \text{ g}^{-1}$ ,

**Table I.** Voltages associated with specific phase transitions between graphite-lithium intercalation compounds, taken from the peaks in the derivative of capacity and of strain with respect to voltage (Fig. 3).

Peak	Transition	Voltage (V vs. $\text{Li}^{+/0}$ )		
		Capacity Derivative*	Strain Derivative*	Capacity Derivative#
A <sub>L</sub>	DI→IV	0.194	0.185	0.195
B <sub>L</sub>	III→DII	0.141	–	0.127
C <sub>L</sub>	DII→II	0.108	0.109	0.107
D <sub>L</sub>	II→I	0.075	0.076	0.060
D <sub>D</sub>	I→II	0.098	0.098	0.107
C <sub>D</sub>	II→DII	0.138	0.139	0.141
B <sub>D</sub>	DII→III	0.174	0.175	0.146
A <sub>D</sub>	IV→DI	0.231	0.218	0.231

\*This work.

#Dahn et al.<sup>2,3</sup> Note, Dahn et al. were unable to associate a specific peak in the capacity derivative with the stage IV to stage III transition.

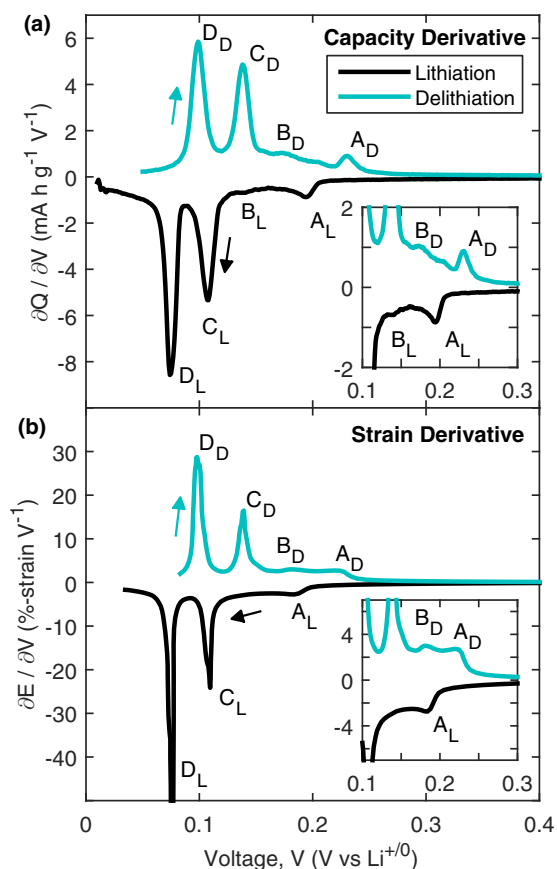


**Figure 3.** Phase transitions between graphite-lithium intercalation compounds. (a) Derivative of capacity with respect to voltage and (b) derivative of strain with respect to voltage of a graphite composite electrode cycled galvanostatically at C/20 rate (third cycle). The derivatives correspond to the electrochemical and mechanical data presented in Fig. 1. The peaks in the derivatives labeled  $A_L$ – $D_L$  and  $A_D$ – $D_D$  correspond to the phase transitions between graphite-lithium intercalation compounds during lithiation and delithiation respectively, which are summarized in Table 1.

manufacturer's specification),  $M_{fg}$  is the mass fraction of graphite in the electrode, and  $M_{f,cb}$  is the mass fraction of carbon black in the electrode. Because the irreversible capacity generated by SEI formation scales linearly with the surface area of the electrode,<sup>20,39</sup> we used these model electrodes to explore the effect of surface area on the irreversible capacity and irreversible strain development in composite electrodes. Fig. 5 shows the cumulative irreversible capacity and cumulative irreversible strain developed in the electrodes during galvanostatic cycling. As expected, the irreversible capacity increased approximately linearly with increased electrode surface area. The irreversible strain also increased with increased electrode surface area, corroborating the correlation of irreversible strain with irreversible capacity. However, the irreversible strain increased non-linearly with increasing electrode surface area. Previous research has shown that the crystallographic structure and surface imperfections of carbon influence the reduction of electrolyte as strongly as surface area.<sup>20,40</sup> Therefore, the SEI that formed on amorphous carbon may be significantly different in composition and structure compared to the SEI that formed on graphitic carbon. We hypothesize that the non-linear relationship between the irreversible strain and the surface area in this study reflects different SEI layers forming on the different types of carbon.

We next systematically varied the cycling rate of composite graphite electrodes with a composition of either 8:1:1 or 9:0:1 graphite, carbon black, and CMC binder. Fig. 6 presents the cumulative irreversible capacity and irreversible strain of the electrodes cycled at C/1 to C/20 rate for three cycles. Smith et al. observed that irreversible capacity increases continuously during galvanostatic cycling, and that total cycling time, rather than cycling rate, is the governing influence on irreversible capacity accumulation.<sup>41</sup> Consistent with their observations, we also observed that the cumulative irreversible capacity increased with increased cycling time, and the irreversible strain followed the same trend.

The similar trends of irreversible capacity and irreversible strain with respect to electrode surface area and cycling time further support the correlation between SEI formation and irreversible electrode deformation. To probe this relationship directly, we subjected graphite composite electrodes to a potentiostatic voltage hold at 0.5 V vs  $\text{Li}^{+/0}$ , below the threshold voltage for electrolyte decomposition but above the threshold for lithiation of graphite. In this test, the capacity gained was directly associated with irreversible electrolyte decomposition

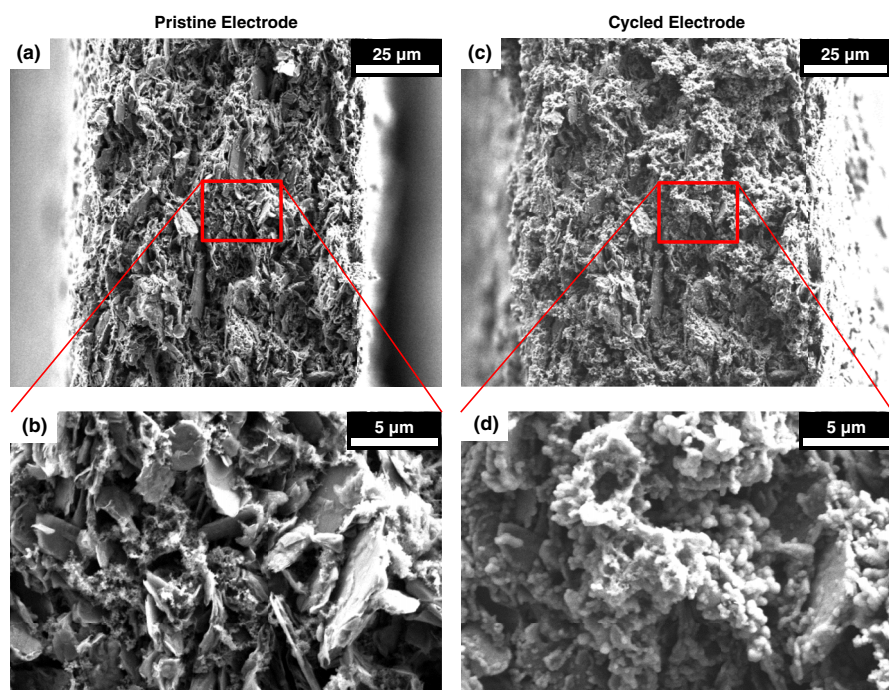


**Figure 4.** Scanning electron micrographs of the edge of a graphite composite electrode before and after electrochemical cycling. The electrode had a composition of 8:1:1 wt ratio of graphite, carbon black, and CMC binder, and was cycled galvanostatically at C/5 rate for five cycles. (a-b) Pristine electrode, before cycling and (c-d) after galvanostatic cycling.

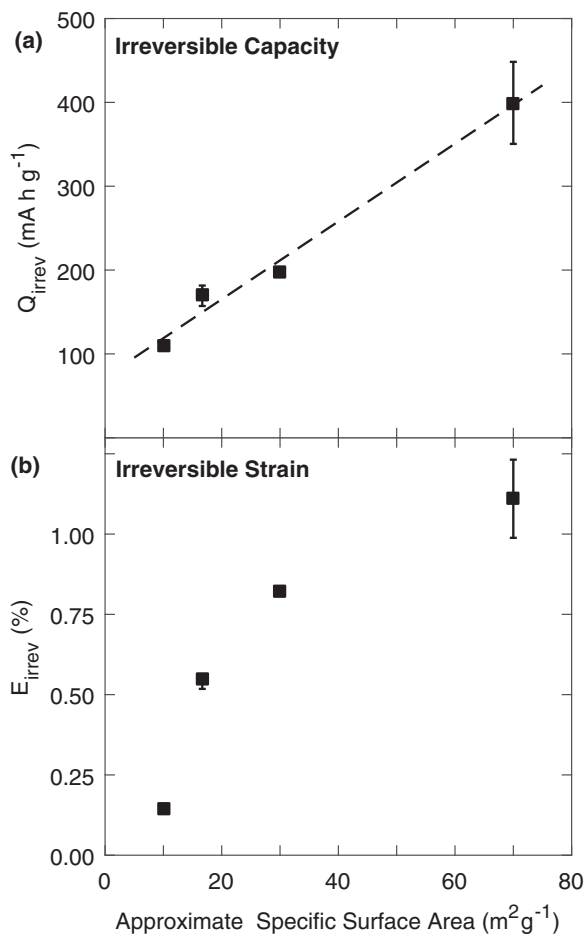


**Figure 5.** Effect of electrically-conductive surface area on the irreversible capacity and strain of graphite composite electrodes during galvanostatic cycling. (a) Irreversible capacity and (b) irreversible strain accumulated during cycles 1–3 at C/5 rate. The irreversible capacity was normalized by the total mass of graphite and carbon black. The approximate specific surface area of the electrically-conductive portion of the electrode was calculated according to Eq. 3. The dashed line in (a) represents a linear fit to the data. Error bars represent the minimum and maximum values of individual tests. Table S1 in the supporting information summarizes the number of tests performed for each composition.

during the formation and growth of the SEI. Representative current, capacity, and strain responses are presented in Fig. 7. The current initially had a large magnitude when the electrode potential was dropped instantaneously from the open circuit potential (ca. 2 V vs Li<sup>+/0</sup>) to 0.5 V vs Li<sup>+/0</sup>. As a result, the capacity increased sharply at the beginning of the voltage hold. The magnitude of the current decreased quickly, but did not approach zero. Therefore, the capacity did not plateau, but continued to increase throughout the voltage hold. Strikingly, the strain response followed the capacity response directly, with a sharp increase at the beginning of the voltage hold and a continual increase during the voltage hold. These results show that electrolyte decomposition directly induces expansion of composite electrodes.

Interestingly, both the capacity and the strain developed during the potentiostatic voltage hold scaled linearly with the square root of time, after initial transient effects, as shown in Fig. 8. Smith et al.<sup>41</sup> also observed a continuous increase in irreversible capacity, proportional to the square root of time, associated with electrolyte decomposition during galvanostatic cycling. Because of the scaling with the square root of time, they attributed the continuous increase of irreversibly capacity to the diffusion of electrolyte components through the SEI layer and subsequent decomposition at the electrode surface.

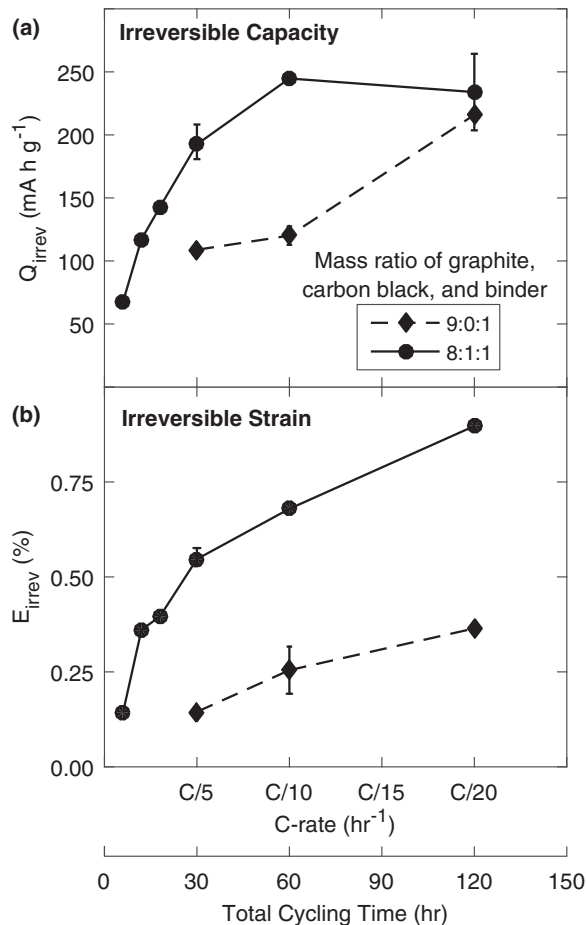


**Figure 6.** Effect of cycling rate/cycling time on the irreversible capacity and strain of graphite composite electrodes during galvanostatic cycling. (a) Irreversible capacity and (b) irreversible strain accumulated during cycles 1–3. Error bars represent the minimum and maximum values of individual tests. Table S1 in the supporting information summarizes the number of tests performed for each composition.

Motivated by the correlation between irreversible capacity and irreversible strain observed during galvanostatic cycling (Fig. 1, Fig. 5 and Fig. 6), the scanning electron micrographs of the SEI layer on a cycled electrode (Fig. 4), and the electrode expansion induced directly by electrolyte decomposition (Fig. 7 and Fig. 8), we postulate that electrolyte decomposition products deposited onto the surface of graphite particles (SEI layer) cause an overall increase in the size of graphite particles, as shown schematically in Fig. 2. This irreversible increase in particle size leads to irreversible macroscopic expansion of the electrode. Using this model, the thickness of the SEI layer can be roughly estimated from the irreversible strain measurements of composite electrodes according to:

$$t = 0.5D_o\varepsilon, \quad [4]$$

where  $t$  is the thickness of the SEI layer,  $D_o$  is the diameter of the pristine graphite particle, and  $\varepsilon$  is the irreversible deformation of the composite electrode. Given a graphite particle size of 10–20  $\mu\text{m}$  and an irreversible deformation of the composite electrode of 1.0%, the thickness of the SEI layer is estimated to be ca. 50–100 nm. These estimations are consistent with experimental X-ray photoelectron spectroscopy measurements of SEI thickness.<sup>22</sup>

In short, formation and growth of the SEI causes irreversible deformation of composite anodes. This conclusion, demonstrated with model, free-standing electrodes, has implications for commercial electrodes, which are adhered to a current collector. In commercial electrodes, constraint from the current collector and battery packaging

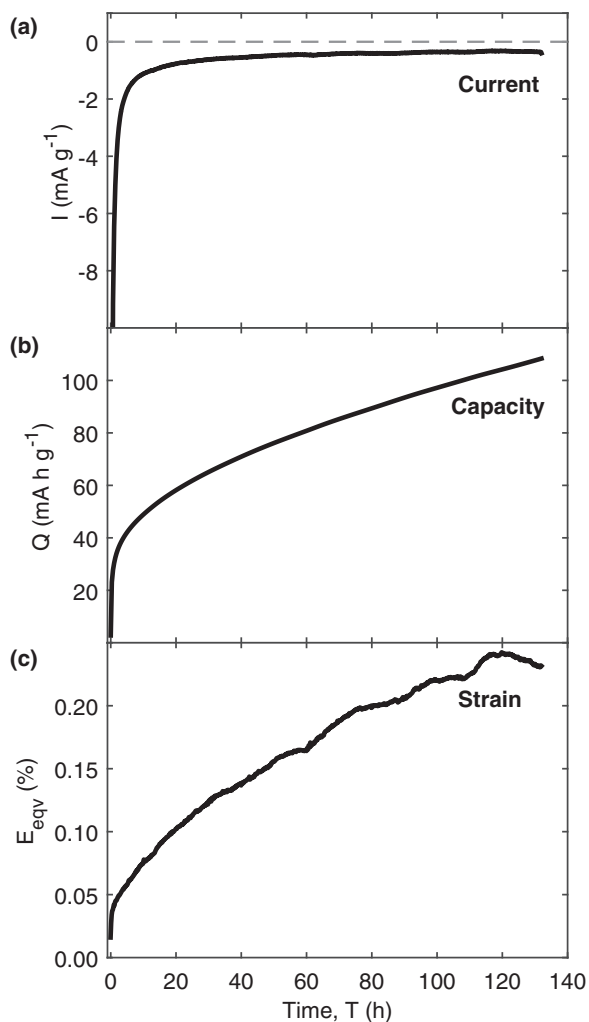


**Figure 7.** Electrochemical and mechanical response of a graphite composite electrode during electrolyte decomposition. The electrode had a composition of 8:1 wt ratio of graphite and CMC binder, and was held at 0.5 V vs  $\text{Li}^{+/0}$  for 132 hours. (a) Current, (b) capacity and (c) strain.

will restrict the free expansion of the electrode during SEI formation, and thus stresses will generate in the electrode, which directly impacts battery performance and lifetime.<sup>9</sup>

**Effect of polymer binder.—Reversible behavior.**—Polymer binders influence the mechanical properties of composite electrodes, such as tensile strength of the electrode and adhesion strength of the electrode to the current collector, and these properties have been investigated previously when the electrodes were outside of a battery environment.<sup>42,43</sup> Here, we explored the effect of polymer binder on the electrochemically-induced deformation of composite graphite electrodes during battery operation. Composite electrodes were fabricated with an 8:1:1 wt ratio of graphite, carbon black, and either carboxymethyl cellulose (CMC) or polyvinylidene (PVdF) binder and were cycled galvanostatically at  $C/5$  rate.

The reversible capacity and strain developed in the electrodes during galvanostatic cycling are presented in Fig. 9a. The electrodes with CMC binder achieved a slightly increased capacity and similar strain compared to the electrodes with PVdF binder. Improved capacity of electrodes made with water-soluble binders such as CMC compared to electrodes made with PVdF binder has been observed previously and has been attributed to better adhesion between binder and active material particles, lower electrical resistance of the composite electrode, and more uniform distribution of binder in the composite electrode.<sup>44</sup>

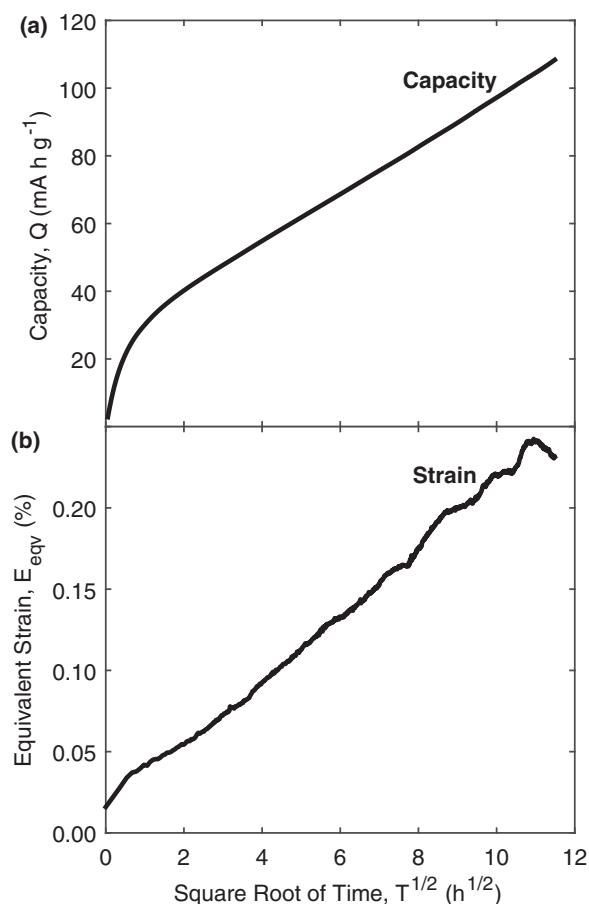


**Figure 8.** Square-root scaling of the electrochemical and mechanical responses of a graphite composite electrode during electrolyte decomposition. (a) Capacity and (b) strain. This is the same data as Fig. 7, but plotted here against the square root of time.

We define the specific expansion of the composite electrode during galvanostatic cycling,  $E_{GS}^s$ , as the reversible electrode deformation induced by a given amount of reversible lithium intercalation/deintercalation:

$$E_{GS}^s = \frac{\Delta E_{ref}}{\Delta Q_{ref}}, \quad [5]$$

where  $\Delta E_{ref}$  is the average reversible strain per cycle and  $\Delta Q_{ref}$  is the average reversible capacity per cycle. The specific expansion ranged between 3.6–4.5 (average 3.9) percent-strain per  $\text{A h g}^{-1}$  for CMC-based electrodes (based on 6 tests) and between 4.2–4.7 (average 4.5) percent-strain per  $\text{A h g}^{-1}$  for PVdF-based electrodes (based on 4 tests). On average, electrodes made with CMC binder expanded approximately 16% less for a given amount of lithium insertion/removal than electrodes made with PVdF binder. This result is consistent with the material properties of the binders themselves: CMC polymer is approximately 20% less compliant than PVdF polymer (Young's modulus of ca. 1.2 GPa for CMC compared to ca. 1.0 GPa for PVdF<sup>45</sup>). We hypothesize that the stiffer CMC binder constrained the electrode more and reduced the macroscopic strain that was developed during electrochemical cycling compared to the more compliant and ductile PVdF binder.

**Irreversible behavior.**—The irreversible capacity and irreversible strain accumulated in the graphite composite electrodes during cycles 1–3 are shown in Fig. 9b. The irreversible capacity of the PVdF-based electrodes was 11% higher than the irreversible capacity for the CMC-based electrodes, while the irreversible strain was 170%

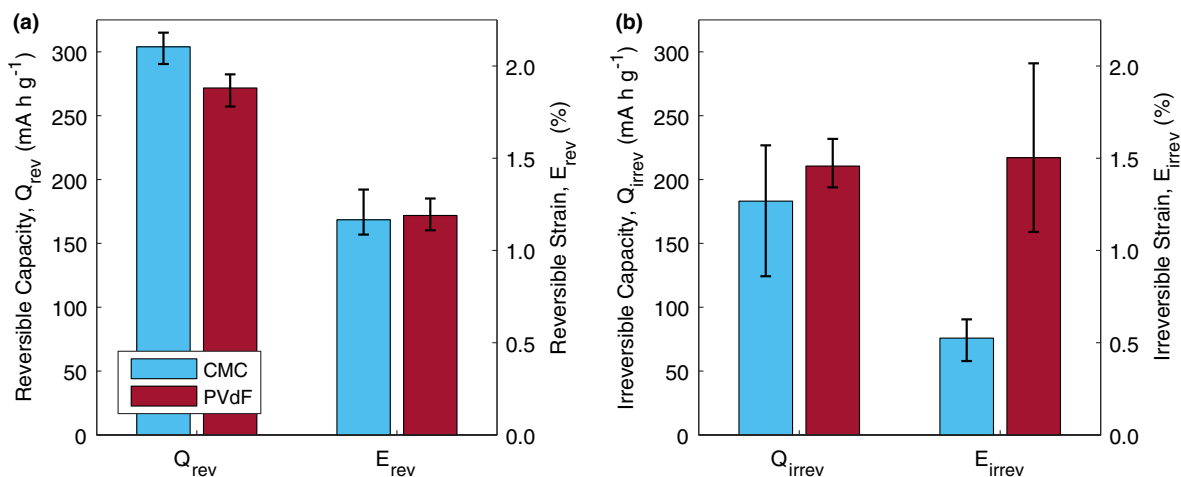


**Figure 9.** Effect of binder on reversible and irreversible electrode behavior. The electrodes had a composition 8:1:1 wt ratio of graphite, carbon black, and polymer binder (either CMC or PVdF), and were cycled at C/5 rate for three cycles. (a) Average reversible capacity and strain and (b) cumulative irreversible capacity and strain. Error bars represent minimum and maximum values of the individual tests (6 tests for CMC-based electrodes and 4 tests for PVdF-based electrodes).

higher. The irreversible capacity results are consistent with previous work that has repeatedly shown higher irreversible capacity for PVdF-based electrodes compared to electrodes made with water-soluble binders such as CMC.<sup>46–48</sup> The large increase in irreversible strain given a moderate increase in irreversible capacity, however, was not expected.

To investigate the effect of polymer binder on the irreversible behavior of electrodes in more depth, we subjected graphite composite electrodes (composition of 8:1 wt ratio of graphite and either CMC or PVdF binder, with no carbon black) to a potentiostatic voltage hold at 0.5 V vs Li<sup>+0</sup>. As mentioned previously, the capacity gained in this test is directly associated with irreversible decomposition of electrolyte solvents during the formation and growth of the SEI. In Fig. 10, the strain is plotted as a function of capacity developed in representative electrodes during the potentiostatic voltage hold.

The potentiostatic experiment revealed an interesting difference in the irreversible behavior of graphite composite electrodes made with the two different binders. When the SEI initially formed (Region I, corresponding to approximately the first 10 minutes of the voltage hold), the CMC-based electrode developed minimal strain while the PVdF-based electrode developed approximately 0.3% strain. During the majority of the potentiostatic test (Region II, corresponding to times greater than approximately 10 minutes), the strain increased linearly with capacity for both the CMC-based electrode and the PVdF-based electrode. The specific expansion of the electrodes during the potentiostatic test,  $E_{PS}^s$ , is defined as:

$$E_{PS}^s = \frac{\Delta E_{II}}{\Delta Q_{II}}, \quad [6]$$

where  $\Delta E_{II}$  is the strain developed in the linear Region II and  $\Delta Q_{II}$  is the capacity developed in the linear Region II. The specific expansion was approximately 2.9 percent-strain per A h g<sup>-1</sup> for CMC-based electrodes and 3.9 percent-strain per A h g<sup>-1</sup> for PVdF-based electrodes. The reduced specific expansion of the CMC-based electrodes compared to PVdF-based electrodes in this linear region was likely due to the lower compliance of the CMC binder itself compared to the PVdF binder. This result is consistent with the reduced specific expansion observed in the reversible electrode deformation during galvanostatic cycling (Reversible behavior section).

We imaged both types of electrodes in a scanning electron microscope before and after potentiostatic voltage hold experiments (Fig. 11). The images of the cycled PVdF-based electrodes clearly reveal a thicker SEI layer compared to the CMC-based electrodes. This visual

evidence is consistent with our strain measurements showing larger electrode expansion due to electrolyte decomposition in PVdF-based electrodes compared to CMC-based electrodes.

We hypothesize that the transition from Region I to Region II of the strain versus capacity response (Fig. 10) indicates a change over time in the nature of decomposition products that formed on the electrode surface. When the electrolyte initially decomposed, the different binders strongly influenced the decomposition reactions and resulting decomposition products, leading to a thicker SEI on the PVdF-based electrodes and therefore larger composite electrode expansion. After an initial SEI was formed over the pristine electrode surface, the binder no longer influenced electrolyte decomposition reactions, and continued SEI growth proceeded in a similar manner for both types of electrodes. While the strain measurements provide the first indication of an evolving SEI, further time-resolved characterization of the SEI composition during extended SEI growth is required to confirm this hypothesis.

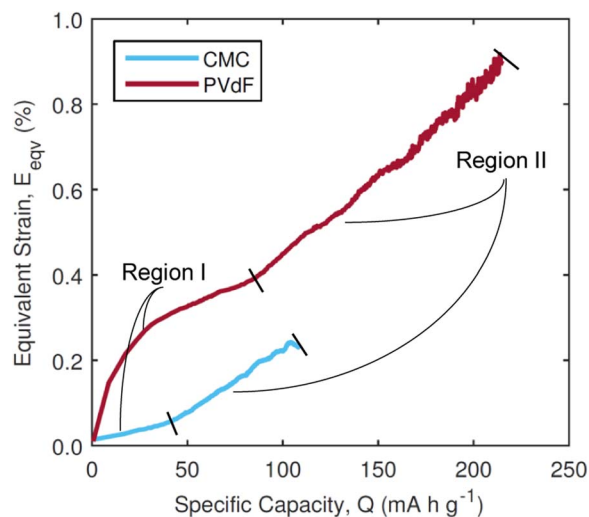


**Figure 10.** Effect of binder on SEI formation and growth. Strain as a function of capacity of graphite composite electrodes during a potentiostatic voltage hold. The electrodes had a composition of 8:1 wt ratio of graphite and polymer binder (either CMC or PVdF), and were held at 0.5 V vs Li<sup>+0</sup>. The CMC-based electrode was held for 132 hours while the PVdF-based electrode was held for 72.5 hours.

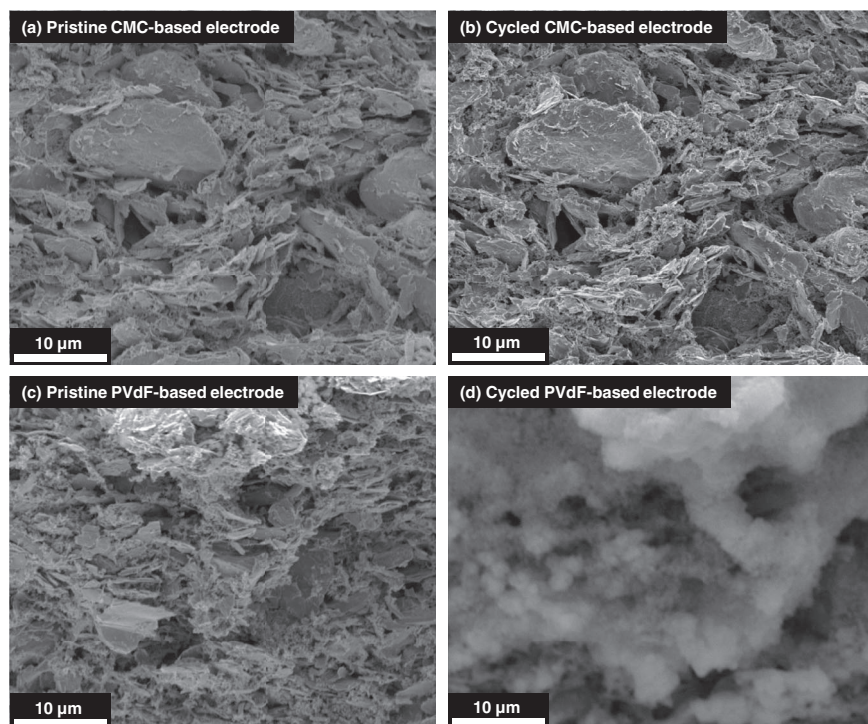


**Figure 11.** Scanning electron micrographs of the edges of graphite composite electrodes fabricated with different binders. The electrodes had a composition of 8:1 wt ratio of graphite and polymer binder (either CMC or PVdF). (a,c) Pristine electrodes and (b,d) electrodes after being held at 0.5 V vs  $\text{Li}^{+/0}$  for 100 hours.

### Conclusions

A more complete understanding of the interplay between electrode mechanics and electrochemical behavior is critical for the improvement of current electrode materials and the development of new high-capacity electrodes for lithium-ion batteries. In this work, we show that changes in graphite layer spacing associated with different graphite-lithium intercalation compounds induce reversible macroscopic expansion/contraction of composite graphite electrodes during galvanostatic cycling. Irreversible electrode deformation is correlated with irreversible electrode capacity, as both increase with increasing electrode surface area and total cycling time. Potentiostatic voltage hold experiments show that the formation and growth of the solid electrolyte interphase (SEI) directly induce macroscopic expansion of graphite composite electrodes. These results strongly suggest that the accumulation of electrolyte decomposition products on the surface of graphite and carbon black particles causes irreversible deformation of electrodes. The choice of polymer binder also influences the electrochemically-induced deformation of composite electrodes. Stiffer binders such as carboxymethyl cellulose (CMC) constrain macroscopic electrode deformation compared to more ductile binders such as polyvinylidene fluoride (PVdF). Additionally, the polymer binder influences the formation and growth of the SEI layer, with a thicker SEI forming on PVdF electrodes, resulting in larger electrode expansion. These results, exemplified here on model electrodes, have significant implications for commercial battery electrodes. Expansion and strain developed in the free-standing electrodes used in this work will be translated directly into stresses in commercial electrodes confined by current collectors and battery packaging. These stresses in turn influence battery performance and lifetime.

### Acknowledgments

This work was supported as part of the Center for Electrochemical Energy Science, an Energy Frontier Research Center funded by the U. S. Department of Energy, Office of Science, Basic Energy Sciences. Dr. Elizabeth Jones acknowledges graduate fellowships through the National Science Foundation and the Beckman Institute for Advanced Science and Technology. The authors also acknowledge the Imaging

Technology Group at the Beckman Institute for use of microscopy equipment, Dr. Joseph Lyding for use of spot welding equipment, Pritam Bhattarai for electrode fabrication, and Anthony Griffin for scanning electron microscopy.

E.M.C.J., N.R.S., and S.R.W. jointly conceived and directed the study, designed the experiments, and interpreted the results. E.M.C.J. performed all electrochemical and strain measurements with subsequent data analysis, performed SEM analysis of CMC-based electrodes before and after electrochemical cycling, created manuscript figures and drafted the manuscript. Ö.Ö.Ç. performed SEM analysis of CMC-based electrodes versus PVdF-based electrodes before and after electrochemical cycling. All authors contributed to editing the final article.

### References

1. K. E. Aifantis, S. A. Hackney, and R. V. Kumar, Current and potential applications of secondary Li batteries, in: *High Energy Density Lithium Batteries*, Wiley-VCH, Weinheim, Germany, 2010, Ch. 4, pp. 81.
2. J. R. Dahn, R. Fong, and M. J. Spoon, Suppression of staging in lithium-intercalated carbon by disorder in the host, *Phys. Rev. B*, **42**(10), 6424 (1990).
3. J. R. Dahn, Phase Diagram of  $\text{Li}_x\text{C}_6$ , *Phys. Rev. B*, **44**(17), 9170 (1991).
4. Y. Qi, H. Guo, L. G. Hector, and A. Timmons, Threefold increase in the Young's modulus of graphite negative electrode during lithium intercalation, *J. Electrochem. Soc.*, **157**(5), A558 (2010).
5. N. Takami, A. Satoh, M. Hara, and T. Ohsaki, Structural and kinetic characterization of lithium intercalation into carbon anodes for secondary lithium batteries, *J. Electrochem. Soc.*, **142**(2), 371 (1995).
6. E. M. C. Jones, M. N. Silberstein, S. R. White, and N. R. Sottos, In situ measurements of strains in composite battery electrodes during electrochemical cycling, *Exp. Mech.*, **54**(6), 971 (2014).
7. Y. Qi and S. J. Harris, In situ observation of strains during lithiation of a graphite electrode, *J. Electrochem. Soc.*, **157**(6), A741 (2010).
8. J. Chen, A. K. Thapa, and T. A. Berfield, In-situ characterization of strain in lithium ion battery anodes, *J. Power Sources*, **271**, 406 (2014).
9. A. Mukhopadhyay and B. W. Sheldon, Deformation and stress in electrode materials for Li-ion batteries, *Progress Mater. Sci.*, **63**, 58 (2014).
10. V. A. Sethuraman, N. Van Winkle, D. P. Abraham, A. F. Bower, and P. R. Guduru, Real-time stress measurements in lithium-ion battery negative-electrodes, *J. Power Sources*, **206**, 334 (2012).
11. A. Mukhopadhyay, A. Tokranov, K. Sena, X. Xiao, and B. W. Sheldon, Thin film graphite electrodes with low stress generation during Li-intercalation, *Carbon*, **49**(8), 2742 (2011).

12. A. Mukhopadhyay, F. Guo, A. Tokranov, X. Xiao, R. H. Hurt, and B. W. Sheldon, Engineering of graphene layer orientation to attain high rate capability and anisotropic properties in li-ion battery electrodes, *Adv. Funct. Mater.*, **23**, 2397 (2013).
13. L. Y. Beaulieu, K. W. Eberman, R. L. Turner, L. J. Krause, and J. R. Dahn, Colossal reversible volume changes in lithium alloys, *Electrochem. Solid-State Lett.*, **4**(9), A137 (2001).
14. X. H. Liu and J. Y. Huang, In situ TEM electrochemistry of anode materials in lithium ion batteries, *Energy Environ. Sci.*, **4**, 3844 (2011).
15. A. Timmons and J. R. Dahn, In situ optical observations of particle motion in alloy negative electrodes for Li-ion batteries, *J. Electrochem. Soc.*, **153**(6), A1206 (2006).
16. V. A. Sethuraman, M. J. Chon, M. Shimshak, V. Srinivasan, and P. R. Guduru, In situ measurements of stress evolution in silicon thin films during electrochemical lithiation and delithiation, *J. Power Sources*, **195**, 5062 (2010).
17. V. A. Sethuraman, A. Nguyen, M. J. Chon, S. P. V. Nadimpalli, H. Wang, D. P. Abraham, A. F. Bower, V. B. Shenoy, and P. R. Guduru, Stress evolution in composite silicon electrodes during lithiation/delithiation, *J. Electrochem. Soc.*, **160**(4), A739 (2013).
18. J. Gonzalez, K. Sun, M. Huang, J. Lambros, S. Dillon, and I. Chasiotis, Three dimensional studies of particle failure in silicon based composite electrodes for lithium ion batteries, *J. Power Sources*, **269**, 334 (2014).
19. D. S. Eastwood, V. Yufit, J. Gelb, A. Gu, R. S. Bradley, S. J. Harris, D. J. L. Brett, N. P. Brandon, P. D. Lee, P. J. Withers, and P. R. Shearing, Lithiation-induced dilation mapping in a lithium-ion battery electrode by 3D X-ray microscopy and digital volume correlation, *Advanced Energy Materials*, **4**, 1 (2014).
20. P. Verma, P. Maire, and P. Novák, A review of the features and analyses of the solid electrolyte interphase in Li-ion batteries, *Electrochim. Acta*, **55**, 6332 (2010).
21. E. Peled, D. Golodnitsky, and J. Penciner, The Anode/Electrolyte Interface, in: *Handbook of Battery Materials*, 2nd Edition, Wiley, 2011, Ch. 16, pp. 479.
22. A. Andersson, A. Henningson, H. Siegbahn, U. Jansson, and K. Edström, Electrochemically lithiated graphite characterized by photoelectron spectroscopy, *J. Power Sources*, **119–121**, 522 (2003).
23. J. Vetter, P. Novak, M. Wagner, C. Veit, K. Möller, J. Besenhard, M. Winter, M. Wohlfahrt-Mehrens, C. Vogler, and A. Hammouche, Ageing mechanisms in lithium-ion batteries, *J. Power Sources*, **147**, 269 (2005).
24. E. Markervich, G. Salitra, M. Levi, and D. Aurbach, Capacity fading of lithiated graphite electrodes studied by a combination of electroanalytical methods, Raman spectroscopy and SEM, *J. Power Sources*, **146**(1–2), 146 (2005).
25. R. Kostecki and F. McLarnon, Microprobe study of the effect of Li intercalation on the structure of graphite, *J. Power Sources*, **119–121**, 550 (2003).
26. L. J. Hardwick, M. Marcinek, L. Beer, J. B. Kerr, and R. Kostecki, An investigation of the effect of graphite degradation on irreversible capacity in lithium-ion cells, *J. Electrochem. Soc.*, **155**(6), A442 (2008).
27. V. A. Sethuraman, L. J. Hardwick, V. Srinivasan, and R. Kostecki, Surface structural disordering in graphite upon lithium intercalation/deintercalation, *J. Power Sources*, **195**(11), 3655 (2010).
28. P. Liu, J. Wang, J. Hicks-Garner, E. Sherman, S. Soukiazian, M. Verbrugge, H. Tataria, J. Musser, and P. Finamore, Aging mechanisms of LiFePO<sub>4</sub> batteries deduced by electrochemical and structural analyses, *J. Electrochem. Soc.*, **157**(4), A499 (2010).
29. S. Bhattacharya, A. R. Riahi, and A. T. Alpas, A transmission electron microscopy study of crack formation and propagation in electrochemically cycled graphite electrode in lithium-ion cells, *J. Power Sources*, **196**(20), 8719 (2011).
30. V. Agubra and J. Fergus, Lithium ion battery anode aging mechanisms, *Mater.*, **6**(4), 1310 (2013).
31. A. Mukhopadhyay, A. Tokranov, X. Xiao, and B. W. Sheldon, Stress development due to surface processes in graphite electrodes for Li-ion batteries: A first report, *Electrochim. Acta*, **66**, 28 (2012).
32. A. Tokranov, B. W. Sheldon, P. Lu, X. Xiao, and A. Mukhopadhyay, The origin of stress in the solid electrolyte interphase on carbon electrodes for Li ion batteries, *J. Electrochem. Soc.*, **161**(1), A58 (2013).
33. H. Tavassol, M. K. Y. Chan, M. G. Catarello, J. Greeley, D. G. Cahill, and A. A. Gewirth, Surface coverage and SEI induced electrochemical surface stress changes during Li deposition in a model system for Li-ion battery anodes, *J. Electrochem. Soc.*, **160**(6), A888 (2013).
34. T. A. Berfield, J. K. Patel, R. G. Shimmin, P. V. Braun, J. Lambros, and N. R. Sottos, Fluorescent image correlation for nanoscale deformation measurements, *Small*, **2**(5), 631 (2006).
35. T. A. Berfield, J. K. Patel, R. G. Shimmin, P. V. Braun, J. Lambros, and N. R. Sottos, Micro and nanoscale deformation measurement of surface and internal planes via digital image correlation, *Exp. Mech.*, **47**, 51 (2007).
36. A. R. Hamilton, N. R. Sottos, and S. R. White, Local strain concentrations in a microvascular network, *Exp. Mech.*, **50**, 255 (2010).
37. D. Guerard and A. Hérol, Intercalation of lithium into graphite and other carbons, *Carbon*, **13**, 337 (1975).
38. T. Utsunomiya, O. Hatozaki, N. Yoshimoto, M. Egashira, and M. Morita, Influence of particle size on the self-discharge behavior of graphite electrodes in lithium-ion batteries, *J. Power Sources*, **196**(20), 8675 (2011).
39. F. Joho, B. Rykart, A. Blome, P. Novák, H. Wilhelm, and M. E. Spahr, Relation between surface properties, pore structure and first-cycle charge loss of graphite as negative electrode in lithium-ion batteries, *J. Power Sources*, **97**, 78 (2001).
40. T. Zheng, A. S. Gozdz, and G. G. Amatucci, Reactivity of the solid electrolyte interface on carbon electrodes at elevated temperatures, *J. Electrochem. Soc.*, **146**(11), 4014 (1999).
41. A. J. Smith, J. C. Burns, X. Zhao, D. Xiong, and J. R. Dahn, A high precision coulometry study of the SEI growth in Li/graphite cells, *J. Electrochem. Soc.*, **158**(5), A447 (2011).
42. J. Chen, J. Liu, Y. Qi, T. Sun, and X. Li, Unveiling the roles of binder in the mechanical integrity of electrodes for lithium-ion batteries, *J. Electrochem. Soc.*, **160**(9), A1502 (2013).
43. W. Haselrieder, B. Westphal, H. Bockholt, A. Diener, S. Höft, and A. Kwade, Measuring the coating adhesion strength of electrodes for lithium-ion batteries, *Int. J. Adhes. Adhes.*, **60**, 1 (2015).
44. S.-L. Chou, Y. Pan, J.-Z. Wang, H.-K. Liu, and S.-X. Dou, Small things make a big difference: binder effects on the performance of li and na batteries, *Phys. Chem. Chem. Phys.*, **16**, 20347 (2014).
45. J. Li, R. B. Lewis, and J. R. Dahn, Sodium carboxymethyl cellulose: a potential binder for Si negative electrodes for Li-ion batteries, *Electrochem. Solid-State Lett.*, **10**(2), A17 (2007).
46. L. Chai, Q. Qu, L. Zhang, M. Shen, L. Zhang, and H. Zheng, Chitosan, a new and environmental benign electrode binder for use with graphite anode in lithium-ion batteries, *Electrochim. Acta*, **105**, 378 (2013).
47. K. Ui, D. Fujii, Y. Niwata, T. Karouji, Y. Shibata, Y. Kadoma, K. Shimada, and N. Kumagai, Analysis of solid electrolyte interface formation reaction and surface deposit of natural graphite negative electrode employing polyacrylic acid as a binder, *J. Power Sources*, **247**, 981 (2014).
48. J.-P. Yen, C.-M. Lee, T.-L. Wu, H.-C. Wu, C.-Y. Su, N.-L. Wu, and J.-L. Hong, Enhanced High-Temperature Cycle-Life of Mesophase Graphite Anode with Styrene-Butadiene Rubber/Carboxymethyl Cellulose Binder, *ECS Electrochem. Lett.*, **1**(6), A80 (2012).